Enhanced Detection of Human-Driven Forest Alterations using Echo State Networks

Tomás Couso Coddou
Department of Computer Science
Pontificia Universidad Católica de Chile
Santiago, Chile
tcouso@uc.cl

Paula Aguirre
Institute of Mathematical Engineering and Computation
Pontificia Universidad Católica de Chile
Santiago, Chile
paaguirr@uc.cl

Rodrigo A. Carrasco
Institute of Mathematical Engineering and Computation & School of Engineering
Pontificia Universidad Católica de Chile
Santiago, Chile
rcarrass@uc.cl

Javier Lopatin
Faculty of Engineering and Sciences
Universidad Adolfo Ibáñez
Santiago, Chile
javier.lopatin@uai.cl

Abstract

Forest monitoring is crucial for understanding ecosystem dynamics, detecting changes, and implementing effective conservation strategies. In this work, we propose a novel approach for automated detection of human-induced changes in woodlands using Echo State Networks (ESNs) and satellite imagery. Using ESNs offers a promising solution for analyzing time-series data and identifying deviations indicative of forest alterations, particularly those caused by human activities such as deforestation and logging. The proposed experimental setup leverages satellite imagery to capture temporal variations in the Normalized Difference Vegetation Index (NDVI) and involves the training and evaluation of ESN models using extensive datasets from Chile's central region, encompassing diverse woodland environments and human-induced disturbances. Our initial experiments demonstrate the effectiveness of ESNs in predicting NDVI values and detecting deviations indicative of human-related changes in woodlands, even in the presence of climate-induced changes like drought and browning. Our work contributes to forest monitoring by offering a scalable and efficient solution for automated change detection in woodland environments. Integrating ESNs with satellite imagery analysis provides valuable insights into human impacts on forest ecosystems, facilitating informed decision-making for sustainable land management and biodiversity conservation.

Tackling Climate Change with Machine Learning: workshop at NeurIPS 2022.

1 Introduction

Monitoring forest ecosystems is crucial for addressing global change and mitigating ecosystem degradation, as forests provide essential services such as water and carbon regulation, nutrient cycling, air purification, biodiversity conservation, climate moderation, and recreational opportunities (16; 19; 20; 2; 4; 7; 32). Deforestation, driven by urbanization and agricultural expansion, leads to the destruction and fragmentation of habitats, disrupting vital ecological functions and threatening biodiversity and sustainable land management (29; 5; 18; 45). While the Amazon rainforest has garnered significant attention, forests worldwide hold immense ecological, economic, and societal value (35; 27; 10).

Natural disturbances such as fires and droughts also contribute to forest degradation, making it challenging to differentiate between deforestation and other forms of degradation (9; 26; 36; 33). Effective landscape management and policy-making require robust monitoring systems that can accurately detect these changes on a large scale, for which remote sensing provides a powerful tool. The time series analysis of optical satellite imagery, combined with machine learning and statistical techniques, has proven effective in detecting landscape changes (38; 25; 17; 44). Notable examples include the Continuous Change Detection and Classification algorithm (CCDC) and Breaks for Additive Season and Trend (BFAST) (46; 43; 24). Deep learning methods have further enhanced our ability to analyze complex, multi-dimensional remote sensing data, with CNNs and RNNs particularly successful in this domain (39; 34; 6).

However, the scalability of CNNs and RNNs remains challenging, particularly regarding computational demands and data requirements (15). Recurrent neural networks (RNNs), despite their ability to model long-term temporal dependencies, face difficulties when adapting to changes in data distribution, a critical factor in dynamic environments like forests (23; 37; 11). In this context, Echo State Networks (ESNs), a type of RNN, offer significant advantages. ESNs can efficiently adapt to new data and predict chaotic time dynamics. Their training process is faster and less prone to the gradient problem compared to other RNNs, as only the readout layer is trained (13; 14; 21; 22; 28). ESNs have been successfully applied in various domains, such as fault detection in industrial systems, yet their application in forest change detection remains underexplored (3; 30).

Our research addresses this gap by developing an ESN-based system for detecting large-scale forest changes, explicitly focusing on central Chile. This region has experienced severe droughts and fires over the past decade, leading to significant tree mortality in a highly heterogeneous landscape of forestry and agricultural mosaics, making it an ideal testing ground for this approach (9; 26).

2 Methods

2.1 Data selection, processing, and training

The study area covers approximately 78,000 km^2 in central Chile (latitudes from -36.5°S to -32.2º S), a region recognized as one of the global biodiversity hotspots (27). Local forests are confronted with anthropogenic pressures such as urbanization, agricultural encroachment, and the introduction of non-native plant species. In the last decade, the region has experienced extreme drought conditions that cause widespread "browning" phenomena (9; 26), and intense wildfire activity, further exacerbating the stress on these vital ecosystems (36).

Our analysis is based on a Landsat multispectral dataset comprising 8,804 scenes captured between January 2000 and June 2022 with the TM, ETM+, and OLI/TIRS sensors aboard Landsat 5, 7, 8, and 9 satellites (41). For each pixel in the study region, we calculated the normalized difference vegetation index (NDVI) (31) using the red and near-infrared bands in each collection and obtained NDVI time series across all observed dates. To address the significant noise and missing values in the raw NDVI signal, we developed a three-step “denoising algorithm" consisting of i)resampling of the NDVI signal to bi-weekly intervals, ii) application of a standard deviation filter with linear interpolation of missing values, and iii)a Holt-Winters exponential smoothing (12).

For training of the change-detection algorithm, we identified areas that likely experienced different forms of deforestation between 2016 and 2022 using records from the Global Forest Watch (GFW) dataset (1). We relied on the visual interpretation of Google Earth Pro imagery for detailed demarcation of degraded polygons. In total, we selected 382 sites. Of these, 142 sites were linked to

	MAPE	MAE	MSE	R^2
non-feedback ESN	0.0671	0.0313	0.0021	0.9115
feedback ESN	0.0732	0.0379	0.0028	0.8462

Table 1: Regression Metrics for non-feedback and feedback ESNs.

human-driven deforestation, while 147 sites corresponded to other changes: 91 areas were affected by the severe drought and vegetation "browning" in the summer of 2019–2020 (26), and 56 sites affected by fires. Additionally, we selected 93 sites with stable time series where no changes occurred. We used pixel-based data for our analyses, resulting in 23,053 individual pixel-based time series across all sites. Further details on the dataset can be found in (8) and in A.3.

2.2 Echo state networks

We trained an Echo State Network (ESN) to predict the expected evolution of the NDVI signal for each pixel. An ESN is a recurrent neural network (RNN) characterized by a reservoir of sparse, randomly initialized, fixed weights (21), in which only the weights to output units are modified for achieving the desired learning task(13). An additional description of an ESN can be found in Appendix A.1. We assume that the generative process underlying the NDVI signal is dynamic since vegetation phenological cycles may vary over time. In such scenarios, an online learning rule like Recursive Least's Squares (RLS) is suitable (21). The ESN training instances consisted of feature-target pairs derived from the NDVI signal. We defined a feature vector of 104 NDVI values (approximately two years of data), with the values of week 105 designated as the target values. This window was then shifted sequentially across the entire time series for each pixel, resulting in 104-dimensional NDVI feature vectors. This process, which we refer to as "signal featurization", involves taking the previous two years for each signal value, so the first target value fed into the net corresponds to the beginning of the third year of available NDVI signal. For training the ESN, we randomly selected 30% of the stable and drought polygons, setting aside the remaining instances to validate the fault detection procedure. Further details on the training procedure are given in A.2.

2.3 Change detection algorithm and model validation

To detect human-driven forest alterations, we adapted the fault detection scheme from (3) to analyze changes in the NDVI time series for each pixel. First, the raw NDVI signal is de-noised and transformed into feature-target pairs of 104 features. Then, the series is divided into two parts: the training section, comprising NDVI values from the beginning of the satellite observations up to a year before the final datum, and the hidden section, which consists of the last value of the signal. The ESN is fine-tuned in the training section and used to predict the hidden section. We refer to this prediction as the signal's reference *lower bound*. Then, the hidden section of the signal is compared to the lower bound using time-shifted predictions. This is achieved by taking a unit from the second section, feeding it into the fine-tuned ESN, and predicting the remaining values. A pixel is classified as *changed* if N consecutive forecasted values of the time-shifted signal are lower than the *lower bound* multiplied by a constant integer k. If no change is detected, the signal is shifted forward by one unit, and the procedure is repeated until a change is detected or no remaining signal is left. We used a voting mechanism to detect changes in entire polygons: a polygon is labeled as changed if the percentage of pixels with a positive flag is greater than or equal to the threshold parameter th.

Appendix A.3 provides detailed information about the ESN dataset used. The data reserved for testing the change detection algorithm encompassed the remaining 70% of the stable and drought polygons (*non change* category), and the complete selection of the fire and drought polygons (*change* category). For each pixel, we used the change detection algorithm with thresholds $th \in \{0.25, 0.5, 0.75\}$, Number of consecutive failures N ranging from 3 to 18 and lower bound coefficient k ranging from 0.8 to 1. The tracked metrics were the Accuracy, the F1-score, the Precision, and the Recall. The details of this analysis can be found in appendix A.3.

3 Results

Table 1 shows the forecasting metrics obtained for both models. Results show that the non-feedback model achieved superior performance, with all error metrics lower than the feedback model and with a higher coefficient of determination.

Figure 1 shows two example polygons before and after the change event, with the algorithm's detection tagged. Appendix A.4 details the tuning parameters used for the detection.

Before event | After event | Detections

Figure 1: Example of fire (top row) and logging (bottom row) polygons. Green dots indicate true positives, while red dots indicate false positives for individual pixels.

Table 2 shows the classification metrics, where an accuracy of 0.708 was achieved. These metrics highlight the model's capacities for capturing true positives, with a recall of 0.823. It is also evident that there is a tendency to incur false positives, with a precision of 0.619. Appendix A.4 has further details on the classification metrics.

To further distinguish the results according to the type of disturbance, we analyzed the classification metrics on four subsets of the polygons according to the type of *non-change* category (stable or drought) and *change* category (logging or fire). Table 3 presents the detailed classification metrics, and reveals an uneven performance across the subsets of polygons. The detection of logging and fire events over stable polygons reached an accuracy of 0.926 and 0.871, respectively, but lower detection scoers are obtained for polygons affected by drought(0.609 for logging and 0.478 for fire). It is noticeable how precision scores rise considerably without the influence of drought-related false positives, with a score of 0.979 for stable polygons and 0.950 for fire.

4 Discussion

The results presented here demonstrate the capabilities of ESNs for capturing forest dynamics and detecting change events in forests. When detecting over stable polygons, ESNs had an overall accuracy of 0.708, 0.926 for fires, and 0.871 for logging events. For polygons affected by drought,

	Precision	**Recall**	**F1-Score**	**Support**
Non change	0.825	0.623	0.710	106
Change	0.619	0.823	0.707	79
Accuracy			0.708	0.708
Macro Avg	0.722	0.723	0.708	185
Weighted Avg	0.737	0.708	0.708	185

Table 2: Classification Metrics for the global model.

Non-Change	Change	Accuracy	F1-Score	Recall	Precision
stable	**logging**	0.926	0.929	0.885	0.979
stable	**fire**	0.871	0.809	0.704	0.950
drought	**logging**	0.609	0.672	0.885	0.541
drought	**fire**	0.478	0.447	0.704	0.328

Table 3: Metrics for different cases of vegetation

the accuracy in change detection was comparatively lower, with a score of 0.609 for logging and 0.478 for fire events.

Our current work focuses on reducing the rate of false positives for drought polygons. One promising venue for this matter is adjusting the change detection criteria. Hence, it considers the prediction error of each particular pixel when determining the extent to which different predicted versus real NDVI values consist of a change in the land cover. Possible ways to implement this are in the change detection criteria defined by (46). Another improvement consists of evaluating the model to detect the precise dates of the events. Doing so frames the problem as one of *Change Point Detection* (CPD), where the objective is to determine time points where a time series changes its state(42). Suitable metrics that can be used for CPD are shown in (42).

Acknowledgments and Disclosure of Funding

Funding

We would like to acknowledge the financial support provided by FONDEF ID21I10102 and FONDECYT 1231245 Grants from ANID. Paula Aguirre also acknowledges funding from CENIA. Tomás Couso Coddou received funding from CENIA to attend the conference.

Competing interests

There are no competing interests to disclose.

References

[1] Global forest watch, 1997.

[2] BOTTALICO, F., TRAVAGLINI, D., CHIRICI, G., GARFÌ, V., GIANNETTI, F., DE MARCO, A., FARES, S., MARCHETTI, M., NOCENTINI, S., PAOLETTI, E., ET AL. A spatially-explicit method to assess the dry deposition of air pollution by urban forests in the city of florence, italy. *Urban Forestry & Urban Greening 27* (2017), 221–234.

[3] CHO, A. D., CARRASCO, R. A., RUZ, G. A., AND ORTIZ, J. L. Slow degradation fault detection in a harsh environment. *IEEE Access 8* (2020), 175904–175920.

[4] DE OLIVEIRA ROQUE, F., MENEZES, J. F., NORTHFIELD, T., OCHOA-QUINTERO, J. M., CAMPBELL, M. J., AND LAURANCE, W. F. Warning signals of biodiversity collapse across gradients of tropical forest loss. *Scientific Reports 8*, 1 (2018), 1–7.

[5] DEFRIES, R. S., RUDEL, T., URIARTE, M., AND HANSEN, M. Deforestation driven by urban population growth and agricultural trade in the twenty-first century. *Nature Geoscience 3*, 3 (2010), 178–181.

[6] DU, B., YUAN, Z., BO, Y., AND ZHANG, Y. A combined deep learning and prior knowledge constraint approach for large-scale forest disturbance detection using time series remote sensing data. *Remote Sensing 15*, 12 (2023).

[7] FIGUEROA, E., AND PASTEN, R. The economic value of forests in supplying local climate regulation. *Australian Journal of Agricultural and Resource Economics 59*, 3 (2015), 446–457.

[8] FUENTES, I., LOPATIN, J., GALLEGUILLOS, M., CEBALLOS-COMISSO, A., EYHERAMENDY, S., AND CARRASCO, R. Is the change deforestation? using time-series analysis of satellite data to disentangle deforestation from other forest degradation causes. *Remote Sensing Applications: Society and Environment* (2024), 101210.

[9] GARREAUD, R. D., BOISIER, J. P., RONDANELLI, R., MONTECINOS, A., SEPÚLVEDA, H. H., AND VELOSO-AGUILA, D. The central chile mega drought (2010–2018): a climate dynamics perspective. *International Journal of Climatology 40*, 1 (2020), 421–439.

[10] HAMILTON, S. E., AND FRIESS, D. A. Global carbon stocks and potential emissions due to mangrove deforestation from 2000 to 2012. *Nature Climate Change 8*, 3 (2018), 240–244.

[11] HUYEN, C. *Designing Machine Learning Systems: An Iterative Process for Production-ready Applications*. O'Reilly Media, Incorporated, 2022.

[12] HYNDMAN, R., AND ATHANASOPOULOS, G. *Forecasting: Principles and Practice*, 2nd ed. OTexts, Melbourne, Australia, 2018. `https://otexts.com/fpp2/` Accessed on 2024-05-01.

[13] JAEGER, H. The "echo state" approach to analysing and training recurrent neural networks. *GMD-Report 148, German National Research Institute for Computer Science* (01 2001).

[14] JAEGER, H., AND HAAS, H. Harnessing nonlinearity: Predicting chaotic systems and saving energy in wireless communication. *Science 304*, 5667 (2004), 78–80.

[15] JEON, W., KO, G., LEE, J., LEE, H., HA, D., AND RO, W. W. Chapter six - deep learning with gpus. In *Hardware Accelerator Systems for Artificial Intelligence and Machine Learning*, S. Kim and G. C. Deka, Eds., vol. 122 of *Advances in Computers*. Elsevier, 2021, pp. 167–215.

[16] KOFINAS, G. P. Adaptive co-management in social-ecological governance. In *Principles of ecosystem stewardship*. Springer, 2009, pp. 77–101.

[17] LARY, D. J., ALAVI, A. H., GANDOMI, A. H., AND WALKER, A. L. Machine learning in geosciences and remote sensing. *Geoscience Frontiers 7*, 1 (2016), 3–10.

[18] LEBLOIS, A., DAMETTE, O., AND WOLFERSBERGER, J. What has driven deforestation in developing countries since the 2000s? evidence from new remote-sensing data. *World Development 92* (2017), 82–102.

[19] LÖF, M., MADSEN, P., METSLAID, M., WITZELL, J., AND JACOBS, D. F. Restoring forests: regeneration and ecosystem function for the future. *New Forests 50*, 2 (2019), 139–151.

[20] LONGO, M., SAATCHI, S., KELLER, M., BOWMAN, K., FERRAZ, A., MOORCROFT, P. R., MORTON, D. C., BONAL, D., BRANDO, P., BURBAN, B., ET AL. Impacts of degradation on water, energy, and carbon cycling of the amazon tropical forests. *Journal of Geophysical Research: Biogeosciences 125*, 8 (2020), e2020JG005677.

[21] LUKOŠEVIČIUS, M. *A Practical Guide to Applying Echo State Networks*. Springer Berlin Heidelberg, Berlin, Heidelberg, 2012, pp. 659–686.

[22] LUKOŠEVIČIUS, M., AND JAEGER, H. Reservoir computing approaches to recurrent neural network training. *Computer Science Review 3*, 3 (2009), 127–149.

[23] LYU, H., LU, H., AND MOU, L. Learning a transferable change rule from a recurrent neural network for land cover change detection. *Remote Sensing 8*, 6 (2016).

[24] MASILIŪNAS, D., TSENDBAZAR, N.-E., HEROLD, M., AND VERBESSELT, J. BFAST lite: A lightweight break detection method for time series analysis. *Remote Sens. (Basel) 13*, 16 (Aug. 2021), 3308.

[25] MCALLISTER, E., PAYO, A., NOVELLINO, A., DOLPHIN, T., AND MEDINA-LOPEZ, E. Multispectral satellite imagery and machine learning for the extraction of shoreline indicators. *Coastal Engineering* (2022), 104102.

[26] MIRANDA, A., LARA, A., ALTAMIRANO, A., DI BELLA, C., GONZÁLEZ, M. E., AND CAMARERO, J. J. Forest browning trends in response to drought in a highly threatened mediterranean landscape of south america. *Ecological Indicators 115* (2020), 106401.

[27] MYERS, N., MITTERMEIER, R. A., MITTERMEIER, C. G., DA FONSECA, G. A., AND KENT, J. Biodiversity hotspots for conservation priorities. *Nature 403*, 6772 (2000), 853–858.

[28] PASCANU, R., MIKOLOV, T., AND BENGIO, Y. On the difficulty of training recurrent neural networks, 2013.

[29] RITCHIE, H., AND ROSER, M. Forests and deforestation. *Our World in Data* (2021).

[30] RODRÍGUEZ-OSSORIO, J. R., MORÁN, A., ALONSO, S., PÉREZ, D., DÍAZ, I., AND DOMÍNGUEZ, M. Echo state networks for anomaly detection in industrial systems. *IFAC-PapersOnLine 56*, 2 (2023), 1472–1477. 22nd IFAC World Congress.

[31] ROUSE JR, J., HAAS, R., SCHELL, J., AND DEERING, D. Paper a 20. In *Third Earth Resources Technology Satellite-1 Symposium: The Proceedings of a Symposium Held by Goddard Space Flight Center at Washington, DC on* (1973), vol. 351, p. 309.

[32] SÁNCHEZ, J. J., MARCOS-MARTINEZ, R., SRIVASTAVA, L., AND SOONSAWAD, N. Valuing the impacts of forest disturbances on ecosystem services: An examination of recreation and climate regulation services in us national forests. *Trees, Forests and People 5* (2021), 100123.

[33] SEBALD, J., SENF, C., AND SEIDL, R. Human or natural? landscape context improves the attribution of forest disturbances mapped from landsat in central europe. *Remote Sensing of Environment 262* (2021), 112502.

[34] SHEN, R., HUANG, A., LI, B., AND GUO, J. Construction of a drought monitoring model using deep learning based on multi-source remote sensing data. *International Journal of Applied Earth Observation and Geoinformation 79* (2019), 48–57.

[35] SILVA JUNIOR, C. H., PESSÔA, A. C., CARVALHO, N. S., REIS, J. B., ANDERSON, L. O., AND ARAGÃO, L. E. The brazilian amazon deforestation rate in 2020 is the greatest of the decade. *Nature Ecology & Evolution 5*, 2 (2021), 144–145.

[36] SMITH-RAMÍREZ, C., CASTILLO-MANDUJANO, J., BECERRA, P., SANDOVAL, N., FUENTES, R., ALLENDE, R., AND ACUÑA, M. P. Combining remote sensing and field data to assess recovery of the chilean mediterranean vegetation after fire: Effect of time elapsed and burn severity. *Forest Ecology and Management 503* (2022), 119800.

[37] SONG, A., CHOI, J., HAN, Y., AND KIM, Y. Change detection in hyperspectral images using recurrent 3d fully convolutional networks. *Remote Sensing 10*, 11 (2018).

[38] THAKUR, S., MONDAL, I., GHOSH, P., DAS, P., AND DE, T. A review of the application of multispectral remote sensing in the study of mangrove ecosystems with special emphasis on image processing techniques. *Spatial Information Research 28*, 1 (2020), 39–51.

[39] TORRES, D. L., TURNES, J. N., SOTO VEGA, P. J., FEITOSA, R. Q., SILVA, D. E., MARCATO JUNIOR, J., AND ALMEIDA, C. Deforestation detection with fully convolutional networks in the amazon forest from landsat-8 and sentinel-2 images. *Remote Sensing 13*, 24 (2021).

[40] TROUVAIN, N., PEDRELLI, L., DINH, T. T., AND HINAUT, X. ReservoirPy: an Efficient and User-Friendly Library to Design Echo State Networks. In *ICANN 2020 - 29th International Conference on Artificial Neural Networks* (Bratislava, Slovakia, Sept. 2020).

[41] USGS. *Landsat 8-9 collection 2 (c2), level 2 science product (l2sp) guide*, 2022. Accessed on 2023-11-13.

[42] VAN DEN BURG, G. J. J., AND WILLIAMS, C. K. I. An evaluation of change point detection algorithms, 2022.

[43] WU, L., LI, Z., LIU, X., ZHU, L., TANG, Y., ZHANG, B., XU, B., LIU, M., MENG, Y., AND LIU, B. Multi-type forest change detection using BFAST and monthly landsat time series for monitoring spatiotemporal dynamics of forests in subtropical wetland. *Remote Sens. (Basel) 12*, 2 (Jan. 2020), 341.

[44] YIN, H., PRISHCHEPOV, A. V., KUEMMERLE, T., BLEYHL, B., BUCHNER, J., AND RADELOFF, V. C. Mapping agricultural land abandonment from spatial and temporal segmentation of landsat time series. *Remote sensing of environment 210* (2018), 12–24.

[45] ZEMP, D., SCHLEUSSNER, C.-F., BARBOSA, H. D. M. J., AND RAMMIG, A. Deforestation effects on amazon forest resilience. *Geophysical Research Letters 44*, 12 (2017), 6182–6190.

[46] ZHU, Z., AND WOODCOCK, C. E. Continuous change detection and classification of land cover using all available landsat data. *Remote Sens. Environ. 144* (2014), 152–171.

A Appendix

A.1 Echo state networks

The reservoir activation vector $x(n)$ is updated according to Equations 1 and 2. At each time step n, the interim activation vector $\widetilde{x}(n)$ is calculated by summing the input vector activation $W^{\text{in}}u(n)$ and the prior activation $Wx(n-1)$, then applying an activation function to the result. Optionally, a feedback layer W^{fb} may also be incorporated to include the previous output vector in the state vector computation. The new activation vector $x(n)$ is subsequently determined through a leaky integration of $\widetilde{x}(n)$ and $x(n)$, with a leaking rate of α. Finally, the output vector $y(n)$ is calculated through the readout layer in Eq. 3.

$$\widetilde{x}(n) = \tanh(W^{\text{in}}u(n) + Wx(n-1) + W^{\text{fb}}y(n-1)) \tag{1}$$
$$x(n) = (1-\alpha)x(n-1) + \alpha\widetilde{x}(n) \tag{2}$$
$$y(n) = W_{\text{out}}[u(n); x(n)] \tag{3}$$

A.2 Training of the echo state network

For training the ESN, we randomly selected 30% of the stable and drought polygons, setting aside the remaining instances for the fault detection procedure. The training dataset of the ESN used the first ten years of instances of each pixel (520 feature-target pairs), roughly 50% of the ESN dataset, and the remaining ten years of values were set aside for testing. We implemented the ESN using the ResevoirPy python library (40). We set the reservoir size to 500 units, the spectral radius 0.9, and the leaking rate to 0.5. We trained two ESN variations in the NDVI forecasting task: a plain-vanilla ESN without feedback connections and an ESN with feedback connections. For validating the trained models, we computed the mean absolute percentage error (MAPE), the mean absolute error (MAE), the mean squared error (MSE), and the coefficient of determination (R^2).

A.3 Data and validation

Table 4 shows the ESN dataset in detail.

Change Type	Number of Polygons	Number of Pixels
Stable	24	780
Drought	27	2405

Table 4: Echo state network training dataset

Table 5 shows the change in the detection task of the dataset in detail, with corresponding labels for each category for the change detection task.

Change Type	Number of Polygons	Number of Pixels	Label
Stable	43	1119	0
Drought	63	4234	0
Logging	52	2064	1
Fire	27	4489	1

Table 5: Change detection dataset, corresponding classification task labels for each category.

A.4 Supplemental Results

Figure 2 shows a grid of F1-scores for our change detection algorithm for all the parameter configurations tested. It can be seen that the best parameters follow a diagonal pattern for all voting thresholds, where lower values of k favored lower values of N, and higher values of k favored higher values of N. The optimal model used the values $th = 0.75$, $N = 3$, and $k = 0.81$, which achieved an F1-score of 0.708.

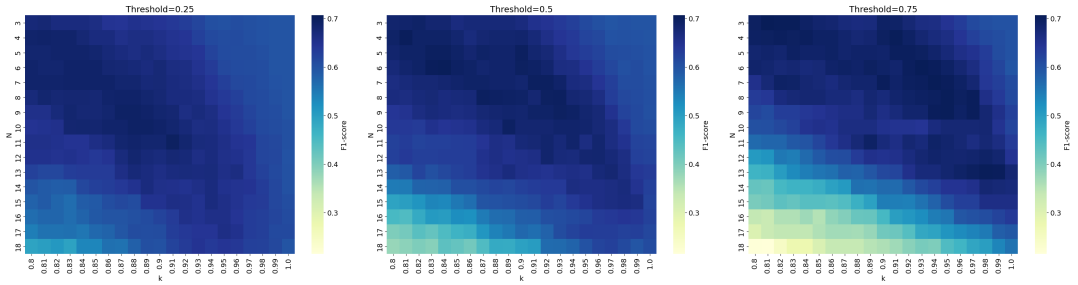

Figure 2: F1-scores for each parameter configuration tested. Darker sections of the grids indicate a higher F1 score, meaning a better balance between Type I and Type II errors.

Table 6 shows the confusion matrix to classifications of the change detection procedure under the optimal parameters. The results are detailed for each possible set of polygons according to the Non-Change and Change categories. It can be seen that the algorithm achieved a high overall performance, with false negatives of only 7.5%. There is a higher tendency for false positives, with a value of 21.6%, which can be explained mainly by mistakes detecting changes in polygons with drought.

		Predicted: Non-Change	**Predicted: Change**
Actual: Non-Change	**Stable**	42 (22.7%)	1 (0.5%)
	Drought	24 (13.0%)	39 (21.1%)
Actual: Change	**Logging**	6 (3.2%)	46 (24.9%)
	Fire	8 (4.3%)	19 (10.3%)

Table 6: Confusion matrix for native vegetation detailed by polygon type.